International Information and Engineering Technology Association
Advancing the World of Information and Engineering

Journal Européen des Systèmes Automatisés
Vol. 59, No. 6, June, 2026, pp. 1649-1664
Journal homepage: http://iieta.org/journals/jesa

Efficiency Improvement of Standalone and Grid-Connected Wind Turbines via Stator Current Optimization Control of a PM Synchronous Generator

Mohammed W. Abdulwahhab[1], Ahmed I. Jaber[1*], A. S. Kaittan[1], D. V. Samokhvalov[2]

[1] Department of Electrical Power and Machine Engineering, College of Engineering, University of Diyala, Diyala 32001, Iraq
[2] Department of Robotics and Automation of Production Systems, Saint Petersburg Electrotechnical University, Saint Petersburg 23803, Russia

Corresponding Author Email: dr.ahmedjaber@uodiyala.edu.iq

https://doi.org/10.18280/jesa.590612

Received: 10 March 2026
Revised: 2 May 2026
Accepted: 11 May 2026
Available online: 30 June 2026

Keywords:
permanent magnet synchronous generator, combined losses, voltage source invertor, OTC control, grid connection

ABSTRACT

Field oriented control (FOC) is one of the most widely used control technologies due to its high efficiency and ability to provide precise dynamic response and improve the performance of electrical systems, especially in wind turbine systems. Classical FOC control utilizes the stator current component q, while the shaft component d is set to zero to achieve maximum torque for non-protruding synchronous machines. However, a system similar to FOC method was developed, called based Stator Current Optimization Control method (OTC). In this system, the torque is modified by the stator current component q, while the value of the shaft component d is negative. This is based on the Flux-Weakening theory of magnetic flux attenuation in the rotor, where the current value of the d component is negative. A true novelty, the combined efficiency, was also achieved. This is the point of equilibrium between the generator and the inverter, meaning that any increase in efficiency in one part of the system is offset by a decrease in the other. As we know, the system consists of several components (generator, inverter, gearbox, and grid) along with control systems. The system was developed using MATLAB Simulink, calculating the total system losses, the efficiency of each component individually and collectively, and calculating the point of equilibrium between the inverter and the generator. These results were then compared with the classical FOC method and the improved method, showing an improvement of up to 4% at low wind speeds and 0.6% at higher wind speeds. Under grid-connected operation, the method maintains total harmonic distortion (THD) below 3% while delivering stable power during wind speed transients. These results confirm that the proposed OTC method enhances both efficiency and grid-compatible power quality.

1. INTRODUCTION

Variable-speed wind turbine systems using permanent magnet synchronous generators (PMSGs) have been widely studied due to their high performance in variable-frequency applications. PMSG provide high efficiency by combining electromagnetic and reactive torque, with wide-range operation using flux-attenuation technology. In this study [1], a wind generator system using an internal PMSG is investigated. PMSG are widely used in many applications as high-performance variable speed drives. In particular, PMSG can offer a highly efficient drive by using reactive torque in addition to magnet torque and provide constant power operation over a wide range using the magnetic flux attenuation method [2]. The optimization of the electromagnetic structure and the control method of the PMSG have attracted significant research interest in recent years. Several methods of controlling the PMSG exist, such as vector control at a given vector current value along the axis ($i_d = 0$), maximum torque per ampere (MTPA), maximum speed per voltage control, loss model control [3-6]. The optimal power search algorithm proposed in this literature [7] maintains peak power points on the power curve. In this research [8], an algorithm for maintaining maximum power based on a neural network is proposed, and in this study [9], an algorithm for maintaining maximum power based on a backpropagation neural network is proposed. However, the control of the PMSG of the surface type is simpler than that of the internal PMSG [10, 11]. Moreover, in many published works, efficiency optimization of PMSG systems has been largely overlooked. In paper [12], the magnetic saturation effect is considered, and the inductance of the internal PMSG along the q axis varies depending on the stator current along the same axis. In addition, in the internal PMSG, the stator current components on both the d and q axis contribute to the developed torque. As a result, the nonlinearity of the system becomes severe if the internal PMSG operates in the flux attenuation region, where the stator current component along the d axis $i_d = 0$. This nonlinearity complicates the direct application of the linear system theory. To solve this problem, non-linear control schemes have been developed to improve the performance of the internal FGM [13].

The minimization of losses in the PMSM core through the suitable design of magnets and grooves, as well as the selection of the number of poles, was investigated in studies [14, 15]. They highlight that in addition to the need for standalone efficiency optimization, the area of connection between wind energy conversion systems (WECS) and the electrical grid introduces new technical requirements, such as power quality, grid synchronization and the regulation of a stable DC-link voltage. The grid-connected inverter is required to transfer active power to the utility grid in the most efficient manner while maintaining a unity power factor, low harmonic distortion, and appropriate responses to grid disturbances [16, 17]. The total harmonic distortion (THD) of grid currents must satisfy international standards such as IEEE 519, which specifies that the THD should not exceed 5% for grid-connected renewable energy system [18]. In this study [19], the authors proposed a maximum power output control method for a variable speed wind turbine system using the PMSG but without closed-loop speed control. Optimal stator current commands on the d and q axes were obtained depending on the generator speed to achieve loss minimization and maximum power maintenance mode. However, since there was no closed-loop speed control, the maximum power point could not be accurately maintained when system parameters changed during actual operation. In addition, the effect of magnetic saturation on the performance, characteristics and control of the PMSM was not considered. In order to achieve optimal efficiency and dynamic response of the CMS, magnetic saturation must be considered when designing the CMS control system for torque and current.

When determining the loss in the generator, the equivalent resistance of the core loss is assumed to be constant [20]. In addition, to avoid DC-bus voltage stability and power quality issues with the grid, the DC-link voltage must not decrease excessively during rapid variations in wind speed [19]. However, for PMSG-based wind turbines many studies have concentrated on maximizing power extraction, but few works have combined this objective with minimizing system losses while also satisfying grid connection requirements. This gap is highly important because flux-weakening control, like many efficiency optimization techniques, can impact the quality of the current waveform and harmonic performance [20]. Thus, it is necessary to validate efficiency-enhancing method under grid-connected conditions to demonstrate its practicality.

To fill this research gap, in contrast to existing studies that mainly focus on the stand-alone mode of proposed respective individual models, the current study evaluates their performance under realistic grid-connected conditions against key metrics including power-tracking accuracy, DC-link voltage stability (total imbalance), grid current synchronization (frequency mismatch), and THD. However, this assumption makes it difficult to accurately determine core loss, as the equivalent resistance varies with rotor speed. To address these challenges, this study examines the effect of losses in the inverter-electrical machine system operating within a wind turbine on the stator current component d-axis. A method is proposed to determine the optimal value of the current component d for energy efficiency, taking into account inverter losses. The current is adjusted according to the rotor rotation speed using the maximum power generation mode linked to wind speed. A wind turbine model is built in Simulink to implement the proposed method and maximize efficiency under both standalone and grid-connected conditions [21]. A comprehensive study was also conducted on the effect of inverter selection on machine losses. More than one inverter was selected to determine its effect. The selection was made by comparing the losses and energy consumption between silicon IGBT and SiC MOSFET chips of different generations. The main conclusion, on which our study was based, was that improving the performance of the electric vehicle does not depend solely on selecting the latest inverter technologies, but the interaction between the inverter, the type of motor, and the entire system must be taken into account [22]. Many recent studies have addressed improving efficiency by taking into account the losses between the inverter and the motor, as in total loss reduction (TLMM), which uses a single method in inverter switching to reduce losses in the generator via the inverter, where the results were compared on one side with a well-known method, the MTPA conventional method [23]. A recent study presented a comprehensive, systematic approach to evaluating the performance of electric vehicles by combining finite element analysis of an interior permanent magnet synchronous motor (IPMSM) with inverter power electronics modeling to assess efficiency and total combined power losses under realistic driving cycles. The results demonstrated that clustering techniques significantly reduced computation time while maintaining high accuracy [24]. A study was conducted to improve the performance of electric vehicles using a multi-motor, multi-gear drive system. The efficiency of both the motor and the inverter (combiner) was analyzed together due to their direct impact on overall vehicle efficiency. A multi-objective optimization model was proposed to refine the drive system design by considering variables such as core length, revolutions per minute, torque distribution, and gear ratios to enhance efficiency and dynamic performance. To reduce computational complexity, an artificial neural network was employed to accelerate the optimization process. The results demonstrate that relying on the integrated efficiency (motor + inverter) achieves better performance than relying solely on motor efficiency. Furthermore, the artificial neural network model significantly reduces computation time while maintaining accurate results [25].

Stator Current Optimization Control method with the current component *d* (OTC) is applied according to the power loss criterion, taking into account losses in the inverter-electrical machine system. The dependence of the efficiency of the PMSG, the inverter, and the overall wind turbine on rotor speed is also studied in both standalone and grid-connected modes. The efficiency results are compared between conventional vector control and the stator current component optimization method, demonstrating improved performance when using the proposed method. The proposed system was modeled using MATLAB/Simulink version (R2018 b) on a personal computer protected by an Intel Core i7 processor and 16 GB of RAM to run Windows 10 programs.

2. SYSTEM MODELING (WIND TURBINE, PMSG, VSI, GEARBOX)

Initially, any design must rely on a complete mathematical analysis, starting with a description of the specific aerodynamics of wind turbines. The mechanical power equation P_t, derived from wind energy, is used. The energy utilization factor C_p *(CMM)*, which is considered in many studies to be the theoretical efficiency of turbines, is then precisely calculated. Since it has a complex mathematical description, it is advisable to use the derived polynomial approximation [26].

$$\begin{cases} P_t = \dfrac{\rho \cdot A_t \cdot v_w^3 \cdot C_p}{2} \\ C_p(\lambda,\beta) = C_1(C_2/\lambda_i - C_3\beta - C_4)^{C_5/\lambda_i} - C_6\lambda \\ \lambda = \dfrac{\omega_t \cdot R}{v_w} \\ \dfrac{1}{\lambda_i} = \dfrac{1}{\lambda + C_7\beta} - \dfrac{C_8}{\beta^3+1} \\ T_t = \dfrac{1}{2\lambda}\rho \cdot A_t \cdot R \cdot {v_w}^2 \cdot C_p(\lambda,\beta) \end{cases} \tag{1}$$

where, P_t is the mechanical power of the turbine (W); v_w is the instantaneous value of the wind speed (m/s), R is the radius of the turbine, m; ω_t is the angular speed of rotation of the turbine shaft, rad/s; ρ is the density of the air (1.225 kg/m^3); A_t is the area of the turbine cross-section through which the wind air flow passes (m^2); λ is the speed factor, $C_p = Pt/Pw$ is the power utilization factor, β is the angle of attack of the turbine blades, $C_1 = 0.5$, $C_2 = 116$, $C_3 = 0.4$, $C_4 = 0$, $C_5 = 5$, $C_6 = 21$, $C_7 = 0.8$, $C_8 = 0.035$ [26] – constants, taking into account the aerodynamic characteristic of the turbine, P_w – wind power, T_t – Torque of the turbine.

Assuming that the phase windings of the PMSG stator have the same resistance and inductance values, and neglecting the losses in the steel (although these losses are taken into account when calculating the total losses of the PMSG), the mathematical model of the PMSG can be expressed as follows [27]:

$$\begin{cases} \dfrac{di_d}{dt} = \dfrac{1}{L_d}\left[v_d - R_s i_d + \omega L_q i_q\right] \\ \dfrac{di_q}{dt} = \dfrac{1}{L_q}\left[v_q - i_d R_s - L_d \omega i_d - \psi_r \omega\right] \\ T_e = \dfrac{3}{2}p\left[\psi_r i_q + \left(L_d - L_q\right) i_q i_d\right] \\ T_e = T_{sh} + J_{tot}\dfrac{d\omega_r}{dt} + B_m \omega_r \\ T_{sh} = \eta_{gear}\dfrac{T_m}{i}, J_{tot} = J_g + \dfrac{J_t}{i^2} \end{cases} \tag{2}$$

where, L_d, L_q are the inductances of the stator winding along the d and q axes, R_s is the resistance of the stator phase windings, i_d, i_q are the projections of the stator current on the d and q axis, v_q, v_d are the voltage projections along the d and q axes, ω is the electric velocity, ω_r is the mechanical rotor rotation speed, ψ_r is the flow coupling of the rotor, p is the number of pairs of poles, T_e is the electromagnetic moment of the PMSG, J_g is the moment of inertia of the generator rotor, B_m is the coefficient of viscous friction, J_t is the moment of inertia of the turbine rotor, $J_{tot.}$ is the total moment of inertia of the turbine rotor and the generator rotor, T_{sh} is the turbine torque reduced to the generator shaft, i is the gearbox ratio, Ƞ *gear* is the efficiency of the gearbox. The mathematical model of the PMSG is built in a rotating coordinate system *d-q,* since it is more convenient when using vector control.

The mathematical model of the voltage source invertor (VSI) was obtained on the basis of the VSI substitution scheme given in this study [16]. As a mathematical model of an autonomous voltage inverter, a system of voltage equations between the emitter and the collector (for a bipolar transistor with an insulated gate) was used, describing the switching process in power semiconductor switches [28]:

$$\begin{cases} V_a = \left[S_a - \dfrac{1}{3}(S_a + S_b + S_c)\right] V_{dc} \\ V_b = \left[S_b - \dfrac{1}{3}(S_a + S_b + S_c)\right] V_{dc} \\ V_b = \left[S_c - \dfrac{1}{3}(S_a + S_b + S_c)\right] V_{dc} \end{cases} \tag{3}$$

where, S_k ($k = a, b, c$) is the switching function. $S_k = 1$ means that the upper arm key is closed and the lower shoulder key is open. where $S_k = 0$, $S_k = 1$ means that the lower shoulder key is closed and the upper shoulder key is open, V_{dc} is the DC link voltage [28]:

$$\begin{cases} L_S \dfrac{di_a}{dt} = \left[V_a - R_S i_a + \dfrac{1}{3}\left(S_b + S_c - 2S_a\right)V_{dc}\right] \\ L_S \dfrac{di_b}{dt} = \left[V_b - R_S i_b + \dfrac{1}{3}\left(S_a + S_c - 2S_b\right)V_{dc}\right] \\ L_S \dfrac{di_b}{dt} = \left[V_c - R_S i_c + \dfrac{1}{3}\left(S_a + S_b - 2S_c\right)V_{dc}\right] \\ C\dfrac{dV_{dc}}{dt} = \left[S_a i_a + S_b i_b + S_c i_c - \dfrac{V_{dc}}{R_L}\right] \end{cases} \tag{4}$$

where, R_s is the resistance of the coils, L_s is the inductance, C is the smoothing capacitor on the DC bus, (i_a, i_b, i_c) and (V_a, V_b, V_c) are the phase currents and voltages. It is worth noting that the model described above is a model of a bipolar transistor with an insulated gate [28].

Grid-side power control active and reactive power injected into the grid are expressed as:

$$P = \frac{3}{2}(v_d i_d + v_q i_q) \tag{5}$$

$$Q = \frac{3}{2}(v_q i_d - v_d i_q) \tag{6}$$

By aligning the dq frame with the grid voltage $v_q = 0$, then:

$$P = \frac{3}{2} v_d i_d \tag{7}$$

$$Q = -\frac{3}{2} v_d i_q \tag{8}$$

where, i_d controls active power, i_q controls reactive power.

3. CONTROL SYSTEM

The turbine is always operated at its maximum power output. The turbine speed is calculated for each wind speed while maintaining a specific speed, called the optimum turbine speed, from which the maximum power output is derived. This optimum speed is calculated using the tip speed ratio (λ_{opt}), which is the rotational speed multiplied by the turbine radius, and the wind speed (v_w). The optimal turbine speed can also be calculated as follows:

$$\omega_{opt} = \frac{\lambda_{opt} \cdot v_w}{R} \tag{9}$$

where, ω_{opt}: The rotational optimal speed of turbine; λ_{opt}: Optimal value of the tip speed ratio. The rotational speed of the wind turbines is also controlled and regulated using the generator's directional control system, by directly controlling the torque on the generator shaft through calculating the optimal electrical load value, which can be calculated using the equation below:

$$\omega_r = \frac{1}{J_{tot}} \int (T_t / i - T_e) \tag{10}$$

A variation in the generator rotor rotational speed causes a corresponding variation in the turbine rotational speed according to the gearbox transmission ratio i, where the turbine speed is expressed as $\omega_t = \frac{\omega_r}{i}$. Consequently, the turbine rotational speed ω_t can be represented as follows:

$$\omega_t = \frac{1}{i \cdot J_{tot}} \int (T_t / i - T_e) \tag{11}$$

In synchronous machines with permanent magnets with an implicit pole rotor, the inductances along the *d* and *q axes* are assumed to be equal to: $L_q = L_d$. J_{tot}- total of moment of inertia, T_e- Electromagnetic torque of PMSG, in this case, the expression for torque can be written as follows:

$$T_e = 1.5p\left[\psi_r i_q\right] \tag{12}$$

Thus, there is a linear relationship between the electromagnetic moment of the PMSG and the current on the *q-axis*, and the value c_t = 1.5 $p\psi_r$ is called the torque coefficient. The transformation of the coordinate system (Clark and Park transformations) for the transition from a three-phase system (abc) to a two-phase fixed coordinate system (α, β system) and a rotating d-q coordinate system is expressed as follows.

$$\begin{cases} i_\alpha = i_a,\ i_\beta = \dfrac{i_b - i_c}{\sqrt{3}} \\ i_d = i_\alpha cos(\theta) + i_\beta sin(\theta) \\ i_q = i_\beta cos(\theta) - i_\alpha sin(\theta) \end{cases} \tag{13}$$

Also, the inverse transformation of coordinate systems, known as the Clarke-Park inverse transformation, is performed for the purpose of transitioning from a d-q rotary coordinate system to a two-phase (α, β) fixed coordinate system and a three-phase (abc) coordinate system, as follows [29].

$$\begin{cases} V_\alpha = V_d\, cos(\theta) - V_q\, sin(\theta) \\ V_\beta = V_\beta\, cos(\theta) + V_d\, sin(\theta) \\ V_a = V_\alpha, V_b = \dfrac{\sqrt{3}}{2}V_\alpha - \dfrac{1}{2}V_\beta \\ V_c = -\dfrac{1}{2}V_\alpha + \dfrac{\sqrt{3}}{2}V_\beta \end{cases} \tag{14}$$

4. LOSS MODELS AND EFFICIENCY DEFINITIONS

To calculate the efficiency of turbines equipped with PMSGs, and to increase the accuracy of the results, we must consider the losses of the gearbox (P_{gear}) and the generator itself. The generator losses are divided into copper losses caused by current and iron losses caused by eddy currents (P_{fe} steel and losses in copper P_{cu}). There are also relatively small mechanical losses, often overlooked by researchers, caused by friction. The losses of the inverter are divided into static and dynamic losses in the transistor and diodes. The gearbox losses are calculated as in the equation below Eq. (15). The gearbox losses are directly proportional to the turbine's rotational speed; any increase in rotation speed increases the gearbox losses.

$$P_{gear} = K_g \cdot P_N \cdot \frac{n_r}{n_{rN}} \tag{15}$$

where, K_g is the coefficient that takes into account the constant losses in the gearbox (for a single-stage planetary gearbox, it is 1.5%), P_N is the rated power of the turbine, n_r is the rotation speed of the turbine rotor, n_{rN} is the nominal rotation speed of the turbine rotor. The efficiency of the gearbox can be determined as follows:

$$\eta_{gear} = \frac{P_t - P_{gear}}{P_t} \cdot 100(\%) \tag{16}$$

The losses of the iron core of a PMSG, which are caused by the phenomena of residual hysteresis and eddy currents, depend on the equivalent core loss resistance R_c. To increase the accuracy of the efficiency calculations of the system in which the losses are to be calculated, researchers must take into account the change in core loss resistance with the rotor speed, as indicated in this study [30-33].

$$R_c = K \cdot \omega \tag{17}$$

$$\begin{cases} P_{cu} = \dfrac{3}{2}R_s \left[\begin{array}{l} \left(I_{od} - \dfrac{\omega L_q I_{oq}}{R_c}\right)^2 \\ + \left(I_{oq} + \dfrac{\omega(\psi_r + L_d I_{od})}{R_c}\right)^2 \end{array} \right] \\ P_{fe} = \dfrac{3}{2}\dfrac{\omega^2}{R_c} \left[\begin{pmatrix} (L_q I_{oq})^2 + \\ (\psi_r + L_q I_{od})^2 \end{pmatrix} \right], P_{mech.} = B_m \cdot {\omega_r}^2 \end{cases} \tag{18}$$

where, $P_{fe}P_{fe}$ iron losses, P_{cu} copper losses, P_{mech} is the mechanical loss in PMSG, I_{od}, I_{oq} are the projections of the magnetization current on the *d* and *q* axes and are determined as follows [31, 32]:

$$\begin{cases} I_{od} = i_d - I_{cd};\ I_{oq} = i_q - I_{cq} \\ I_{cd} = -\left(\dfrac{L_q}{R_c}\right)\omega I_{oq} \\ I_{cq} = \left(\dfrac{1}{R_c}\right)(\psi_r + L_d I_{od})\omega, \\ I_{od} = i_d + \dfrac{L_q}{R_c}\omega I_{oq} \\ I_{oq} = i_q - \dfrac{1}{R_c}(\psi_r + L_d I_{od})\omega \end{cases} \tag{19}$$

where, I_{cd}, I_{cq} are the components of the loss current in steel along the axes *d*, *q*, *ω*- rotor speed.

The efficiency of the PMSG can be determined as follows:

$$\eta_{PMSG} = \frac{\left(P_t - P_{gear}\right) - \left(P_{cu} + P_{fe} + P_{mech}\right)}{\left(P_t - P_{gear}\right)} \cdot 100(\%) \tag{20}$$

VSI losses are divided into dynamic (switching) and static (conductivity) losses, which mainly depend on the switching characteristics and conduction behavior of the semiconductor devices. These losses are determined separately according to the operating conditions and device parameters as follows [32]:

$$\begin{cases} P_{s.L} = \dfrac{6}{\pi} \cdot f_s \cdot \left(E_{on,I} + E_{off,I} + E_{\text{off,D}}\right) \cdot \dfrac{V_{dc}}{V_{ref.}} \cdot \dfrac{I_L}{I_{ref.}} \\ P_{cond,I} = \dfrac{V_{CE,0}}{2\pi} \cdot I_L \cdot \left(1 + \dfrac{M \cdot \pi}{4} \cos(\phi)\right) \\ + \dfrac{r_{CE,0}}{2\pi} \cdot \left(\dfrac{\pi}{4} + M\left(\dfrac{2}{3} \cdot \cos(\phi)\right)\right) \\ P_{cond,\text{D}} = \dfrac{V_{F,0}}{2\pi} \cdot I_L \cdot \left(1 - \dfrac{M \cdot \pi}{4} \cos(\phi)\right) \\ + \dfrac{r_{CE,0}}{2\pi} \cdot \left(\dfrac{\pi}{4} - M\left(\dfrac{2}{3} \cdot \cos(\phi)\right)\right) \end{cases} \tag{21}$$

where, $P_{s.L}$ is the dynamic loss of the transistor, $P_{cond,I}$ is the static loss of the transistor, $P_{cond,D}$ is the static loss of the diode, I_L is the maximum value of the AC amplitude, M is the modulation index of the PWM [30], ϕ is the angle between the PWM voltage and the linear current, f_s is the frequency of the PWM.

To calculate the power losses in the inverter, the relevant transistor and diode parameters employed for this loss determination are summarized in Table 1 below, with the device characteristics drawn from reference [34].

Table 1. Specifications adopted for the simulated voltage source inverter (VSI) [34]

Parameters	Symbols	Rating Values
Voltage between collector and emitter	$V_{CE,0}$	1.8 V
Collector voltage	V_{ref}	390 V
Transistor resistance in the open state	R_{ce}	0.06 Ω
Transistor turn-on losses	$E_{on,I}$	470 × 10^{-3} mJ
Transistor turn-off losses	$E_{off,I}$	1.8 mJ
Diode losses	$E_{off,D}$	590 µJ
Collector current	I_{ref}	30 A
Forward voltage when the transistor is open	$V_{F;0}$	1.8 V

VSI efficiency is determined as follows:

$$\eta_{VSI} = \frac{\left(P_t - P_{gea\kappa} - P_{cu} - P_{fe} - P_{mech}\right) - \left(Ps.L + Pcond,I + Pcond,D\right)}{\left(P_t - P_{gear} - P_{cu} - P_{fe} - P_{mech}\right)} \cdot 100(\%) \tag{22}$$

Total losses of a wind turbine ($P_{tot.}$) and the overall efficiency of a wind turbine are determined as follows [30]:

$$P_{tot.} = P_{gear} + P_{fe} + P_{cu} + P_{mech} + P_{Ps.L} + P_{cond,I} + P_{cond,D} \tag{23}$$

$$\eta = \eta_t \cdot \eta_{gear} \cdot \eta_{VSI} \cdot \eta_{PMSG} \cdot \frac{P_t - P_{tot.}}{P_t} \tag{24}$$

where, η is the total efficiency of the wind turbine, η_t is the turbine efficiency (CMM C_p), η_{PMSG} is the efficiency of the PMSG, η_{VSI} is the efficiency of the inverter.

As mentioned previously, to calculate and determine the relationship between overall efficiency and speed, the losses in each part of the system are calculated (turbine, permanent magnet generator, gearbox, VSI).

5. PROPOSED OTC CONTROL STRATEGY

Electromagnetic losses P_{EM} in fixed magnet generators (PMSG) consist of a combination of magnetic losses in the steel (P_{fe}) and electrical losses in the form of copper losses (P_{cu}). As shown in the equation below:

$$P_{EM} = P_{cu} + P_{fe} \tag{25}$$

Copper losses, iron losses and mechanical losses due to friction of the generator can also be calculated using the equations shown below. These equations provide a quantitative estimation of the main loss components in the generator, allowing the contribution of each loss mechanism to the total power loss to be evaluated.

$$\begin{cases} P_{cu} = \dfrac{3}{2} R_s \left[\left(I_{od} - \dfrac{\omega L_q I_{oq}}{R_c}\right)^2 + \left(I_{oq} + \dfrac{\omega(\psi_r + L_d I_{od})}{R_c}\right)^2 \right] \\ P_{fe} = \dfrac{3}{2} \dfrac{\omega^2}{R_c} \left[\left(\left(L_q I_{oq}\right)^2 + \left(\psi_r + L_q I_{od}\right)^2 \right) \right] \\ P_{mech.} = B_m \cdot {\omega_r}^2 \end{cases} \tag{26}$$

where, P_{mech} – mechanical losses in the PMSG; I_{od}, I_{oq} – are the magnetizing currents on the d and q axes; L_d, L_q – inductances of the stator windings along d, q axes; R_s–is the stator resistance; R_c – equivalent core-loss resistance; ω – is the electrical speed; ω_r – is the mechanical rotor speed; ψ_r – the rotor flux linkage; B_m – coefficient of viscous friction; T_e – electromagnetic torque of PMSG.

Using Eq. (26), it is possible to express the electrical losses specific to electric generators as a function of ω, I_{od}, and I_{oq}. At steady state, the electromagnetic losses of a PMSG also depend on the value of I_{od}. For a PMSG with a non-salient rotor, $L_d = L_q$. The optimal value of the current component along the d-axis can also be determined by setting the first derivative of the electrical losses with respect to I_{od} to zero, to determine the optimal stator current (I_{od}) according to the minimum electrical losses' criterion for a PMSG.

The negative d-axis current (I_d) is represented by a weakening of the rotor magnetic flux of the generator, which reduces the total flux along the d-axis and allows the generator to operate at higher speeds compared to the case where $I_d = 0$. This process also reduces the flux coupling resulting from the weak flux, which reduces iron losses. The optimum value of the stator current component along the q-axis (I_{oq}) to achieve the maximum electromagnetic torque of the PMSG generator can be determined as follows.

$$\begin{gathered}\frac{dP_{EM}}{dI_{od}} = \psi_r^3 \cdot \left(\frac{3}{2}\cdot\frac{P}{2}\right)^2 \cdot I_{od}\left(R_s R_c^2 + \omega^2 L_d^2 R_s + \omega^2 L_d^2 R_c\right) + \psi_r^4 \cdot \left(\frac{3}{2}\cdot\frac{P}{2}\right)^2 L_d (R_s + R_c)\omega^2 \\ при\ \frac{dP_{EM}\left(I_{od}, I_{oq}, \omega\right)}{dI_{od}} = 0 \Rightarrow I_{od} = -\frac{\psi_r (R_s + R_c)\omega^2 L_d}{R_s R^2{}_c + \omega^2 L_d^2 (R_s + R_c)}\end{gathered} \tag{27}$$

$$I_{oq}^* = \frac{\left(R_s R^3{}_c + \omega^2 L_d^2 (R_s R_c + R^2{}_c)\right) I_q - \psi_r \omega\left(1 + L_d^2 (R_s + R_c)\right)}{R_s R^3{}_c + \omega^2 L_d^2 (R_s R_c + R^2{}_c)} \tag{28}$$

where, I_d, I_q – d, q axis currents.

Inverter losses (VSI) can be divided into dynamic switching losses and static conduction losses, and can be calculated using the following equations [14, 31, 32, 35, 36]:

$$\begin{cases} P_{s.L} = \dfrac{6}{\pi}\cdot f_s \cdot \left(E_{on,I} + E_{off,I} + E_{\text{off,D}}\right)\cdot \dfrac{V_{dc}}{V_{ref.}}\cdot\dfrac{I_L}{I_{ref.}} \\ P_{cond,I} = \dfrac{V_{CE,0}}{2\pi}\cdot I_L \cdot \left(1 + \dfrac{M\cdot\pi}{4}\cos(\phi)\right) + \\ \dfrac{r_{CE,0}}{2\pi}\cdot\left(\dfrac{\pi}{4} + M\left(\dfrac{2}{3}\cdot\cos(\phi)\right)\right) \\ P_{cond,\text{D}} = \dfrac{V_{F,0}}{2\pi}\cdot I_L \cdot \left(1 - \dfrac{M\cdot\pi}{4}\cos(\phi)\right) + \\ \dfrac{r_{CE,0}}{2\pi}\cdot\left(\dfrac{\pi}{4} - M\left(\dfrac{2}{3}\cdot\cos(\phi)\right)\right) \\ P_{VSI} = P_{s.L} + P_{cond,I} + P_{cond,\text{D}} \end{cases} \tag{29}$$

where, f_s is the VSI switching frequency, V_{dc} is the DC link voltage, I_L is the peak amplitude of the sinusoidal AC line current, $E_{on,I}$ and $E_{off,I}$ are the IGBT turn-on and turn-off energies, $E_{off,D}$ is the power diode turn-off energy due to reverse recovery current, $P_{cond,I}$ represents the transistor's static losses, and $P_{cond,D}$ represents the diode's static losses. Because inverter losses are influenced by the stator current, selecting the calculated optimal current value will directly impact these losses. Taking this into account, it is essential to establish how the inverter losses vary. The sum of losses in both the inverter and the PMSG is referred to as the combined losses. The relationship between the total losses and the stator current along the d-axis (I_{od}) can be determined using Eqs. (25) and (29):

$$P_{comb} = P_{EM} + P_{VSI} \tag{30}$$

Eq. (5) allows us to determine how the total losses in the inverter-machine system depend on the Iod current, taking into account the electromagnetic losses in the machine ($P_{cu} + P_{fe}$). The minimum total loss function is achieved when the following condition is met:

$$\begin{aligned} & P_{comb} = P_{EM} + P_{VSI} \\ & P_{comb} = \\ & \left(\frac{3}{2}R_s\left[\left(I_{od} - \frac{\omega L_q I_{oq}}{R_c}\right)^2 + \left(I_{oq} + \frac{\omega\left(\psi_r + L_d I_{od}\right)}{R_c}\right)^2\right] + \frac{3}{2}\frac{\omega^2}{R_c}\left[\left(\begin{array}{l}\left(L_q I_{oq}\right)^2 \\ +\left(\psi_r + L_q I_{od}\right)^2\end{array}\right)\right]\right) + \\ & \left(\begin{array}{l}\dfrac{6}{\pi}\cdot f_s\cdot\left(E_{on,I} + E_{off,I} + E_{\text{off,D}}\right)\cdot\dfrac{V_{dc}}{V_{ref.}}\cdot\dfrac{I_L}{I_{ref.}} + \dfrac{V_{CE,0}}{2\pi}\cdot I_L\cdot\left(1 + \dfrac{M\cdot\pi}{4}\cos(\phi)\right) \\ + \dfrac{r_{CE,0}}{2\pi}\cdot\left(\dfrac{\pi}{4} + M\left(\dfrac{2}{3}\cdot\cos(\phi)\right)\right) + \dfrac{V_{F,0}}{2\pi}\cdot I_L\cdot\left(1 - \dfrac{M\cdot\pi}{4}\cos(\phi)\right) + \\ \dfrac{r_{CE,0}}{2\pi}\cdot\left(\dfrac{\pi}{4} - M\left(\dfrac{2}{3}\cdot\cos(\phi)\right)\right)\end{array}\right) \end{aligned} \tag{31}$$

The rate of change of electromagnetic losses in the machine with respect to the current component along the *d*-axis can be calculated.

$$P_{EM} = \frac{3}{2}R_s\left[\left(I_{od} - \frac{\omega L_q I_{oq}}{R_c}\right)^2 + \left(I_{oq} + \frac{\omega(\psi_r + L_d I_{od})}{R_c}\right)^2\right] + \frac{3}{2}\frac{\omega^2}{R_c}\left[\begin{pmatrix}\left(L_q I_{oq}\right)^2 \\ +\left(\psi_r + L_q I_{od}\right)^2\end{pmatrix}\right]$$
$$\frac{dP_{EM}}{dI_{od}} = 3R_s\left[\left(I_{od} - \frac{\omega L_q I_{oq}}{R_c}\right) + \frac{I_{oq} L_d \omega}{R_c} + \left(\frac{L_d\omega^2}{R_c}\frac{\psi_r}{R_c} + \frac{L_d\omega^2}{R_c}\frac{L_d I_{od}}{R_c}\right)\right]$$
$$+3\frac{\omega^2}{R_c}\left[\left(\psi_r + L_q I_{od}\right)L_q\right] = \frac{dP_{EM}}{dI_{od}} =$$
$$\left(3R_s + 3R_s\frac{L_d^2\omega^2}{R_c^2} + 3\frac{\omega^2}{R_c}L_q L_q\right)I_{od} + 3R_s\frac{\psi_r L_d\omega^2}{R_c^2} + 3\frac{\omega^2}{R_c}L_q\psi_r \tag{32}$$

$$\frac{dP_{VSI}}{dI_{od}} = \frac{I_{od}}{\sqrt{I_{od}^2 + I_{oq}^2}}\begin{bmatrix}\frac{6}{\pi}\cdot f_s\cdot\begin{pmatrix}E_{on,I} + \\ E_{off,I} \\ +E_{off,D}\end{pmatrix}\frac{V_{dc}}{I_{ref}.V_{ref.}}\frac{V_{CE,0}}{2\pi}\left(1 + \frac{M\cdot\pi}{4}cos(\phi)\right) \\ +\frac{V_{F,0}}{2\pi}\cdot\left(1 - \frac{M\cdot\pi}{4}cos(\phi)\right)\end{bmatrix} \tag{33}$$

In the same way, and based on Eq. (4), the rate of change of electrical losses in the inverter with respect to the current component along the *d*-axis is calculated.

The rate of change of total losses depends on the calculated value of the current I_{od}, taking into account the effect of rotor field attenuation, according to the following formula.

$$\frac{dP_{comb}}{dI_{od}} = \frac{dP_{EM} + dP_{VSI}}{dI_{od}} \tag{34}$$

The algorithm of calculating the total efficiency, which combines all parts of this system including the proposed control method, can be seen in Figure 1.

The overall efficiency calculation algorithm, which integrates all components of this system, including the proposed control method, is shown in Figure 1 below. This diagram illustrates the integrated methodology for modeling and optimizing the efficiency of a wind energy conversion system (WECS) based on a PMSG with a voltage source transformer (VSI). It considers system losses in all components and ensures no losses are neglected. The process begins by determining the incoming wind speed (v_w) and constructing a complete wind turbine model using MATLAB Simulink. This model relies on dynamic and geometric parameters of the turbine, such as blade radius, through-air density, and power factor, which represents the turbine's efficiency according to Betzi's law. The PMSG model is then developed using standardized data and its electrical and mechanical parameters, based on real data from a well-known global brand of motors. Finally, key operational variables such as the axial currents (d and q) and angular velocity are measured. This work incorporates gearbox losses and their significant impact on the accuracy of the results. It also models the VSI transformer, defining control parameters and connection and switching losses. During the optimization phase, copper and iron losses in the PMSG are reduced by adjusting the d-axis current, while VSI performance is improved by assessing power losses and determining optimal operating values. Finally, the efficiencies of both the PMSG and VSI are calculated separately, and the results are combined to obtain the overall system efficiency, enabling a comprehensive evaluation and effective optimization of the entire wind power system. The control diagram of a PMSG with classical vector control without using the rotor field weakening method (Field oriented control (FOC) when I_{od} = 0) and using the rotor field weakening method (OTC when I_{od} < 0) (stator current optimization method of a PMSG with vector control) with grid side, is shown in Figure 2.

Figure 2 illustrates the integrated operating architecture and control circuitry for the turbine and generator, as well as the grid control, of a wind turbine conversion system based on a PMSG connected to the electrical grid via a back-to-back AC-AC converter to achieve high operational efficiency. The wind turbine extracts kinetic energy from the wind and converts it into mechanical energy, which is then transferred through a gearbox to the generator. The generator produces electrical power with varying voltage and frequency depending on the wind speed. The generator side employs maximum power point tracking (MPPT) and two methods of current optimization—the classic FOC method and the OTC method—to ensure maximum power extraction while minimizing electrical losses through precise regulation of the shaft currents (*dq*) and to determine the optimal method for maximizing efficiency. The generated power is then stabilized via a DC-link before the grid side regulates the DC-link voltage, controls the active and reactive power, and synchronizes with the grid using PLL technology. This integrated structure ensures improved overall system efficiency, reduced losses in the generator and transformers, and high stability and reliability in pumping power to the grid under various operating conditions.

The power is stored in the DC-Link capacitor to provide voltage stability, and the current then passes to the grid-side converter (GSC), which converts the DC voltage back into a three-phase AC that is synchronized with the grid using a DC-AC voltage source converter and spatial pulse width modulation (SVPWM) technology. The system has active and reactive power control (P and Q) through PI and PLL control panels for phase synchronization, with LCL filters to ensure the quality of the voltage output to the 300 V electrical grid at 50/60 Hz, enabling bi-directional power flow between the generator and the grid. This scheme is implemented using the visual modeling environment for dynamic systems Simulink and is shown in Figure 3.

The scheme implements a model of an autonomous wind energy conversion system on the basis of a PMSG with vector control based on SVPWM, taking into account the power losses and efficiency of the gearbox and the mechanical losses of the PMSG, power losses and the VSI losses. The maximum power tracking mode operates in the range of specified wind speed values (from 5 to 15 m/s) and gear ratio i = 3.

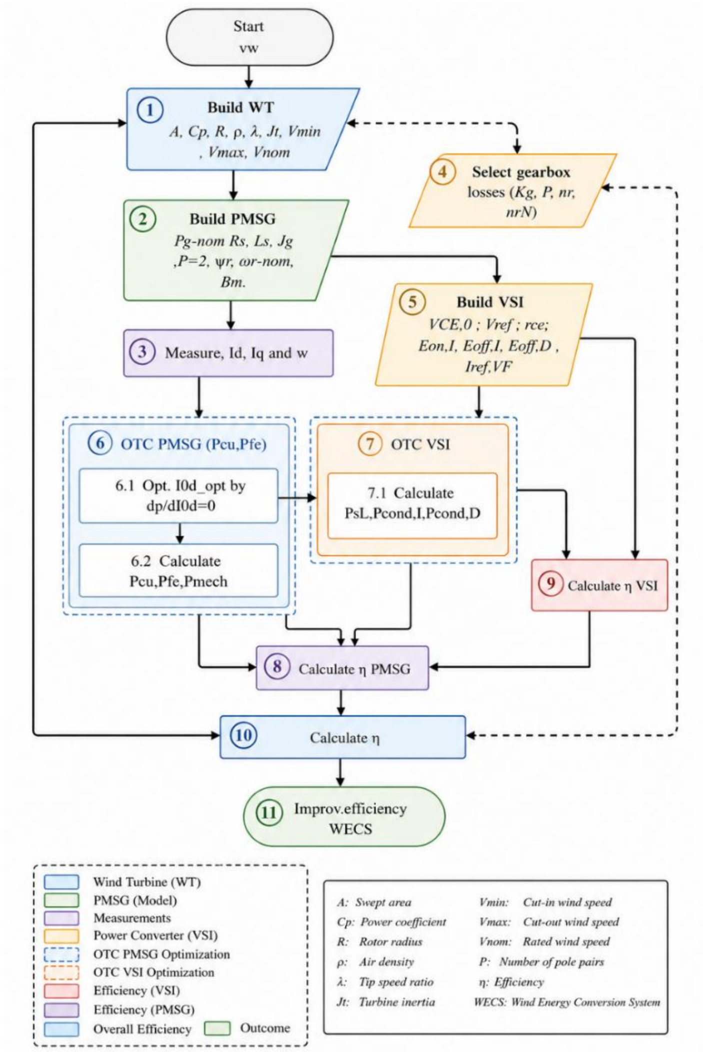

Figure 1. Algorithm of improving the total efficiency

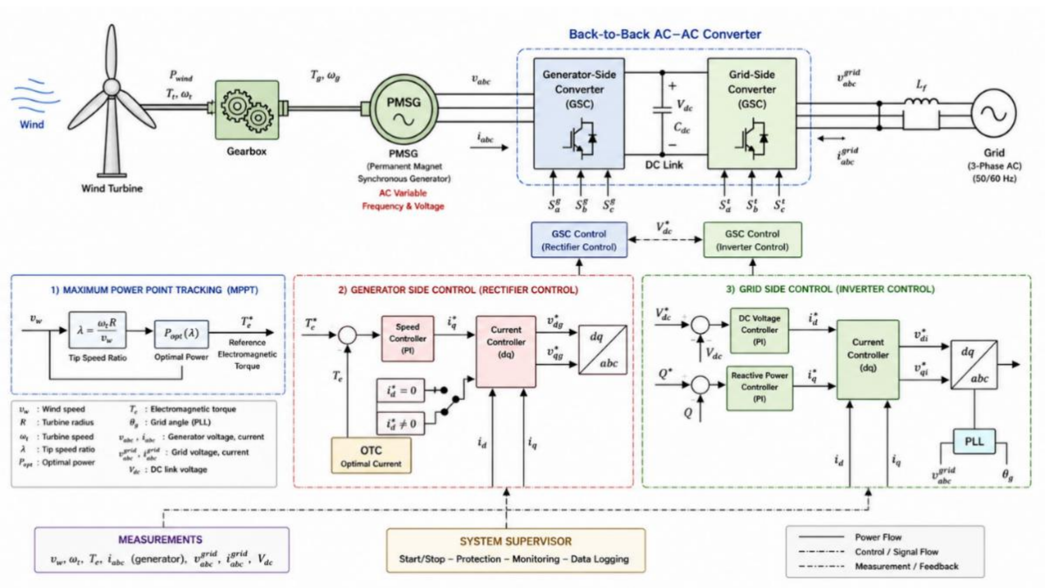

Figure 2. Block diagram of standalone and grid control systems with maximum power point tracking (MPPT) based Stator Current Optimization Control method (OTC), classical vector control field oriented control (FOC)

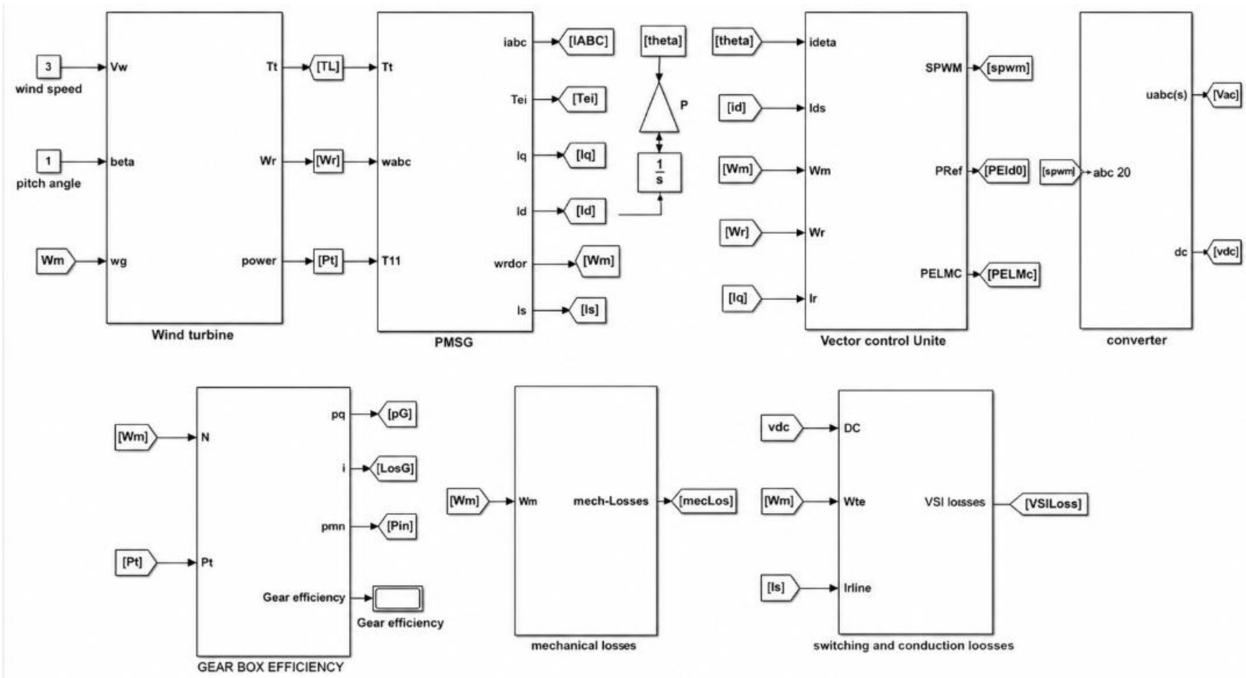

Figure 3. Model of an autonomous wind energy conversion system based on permanent magnet synchronous generator (PMSG) with Stator Current Optimization Control method (OTC) method

6. SIMULATION RESULTS

6.1 Simulation setup and conditions

Simulations were carried out for 30 seconds using MATLAB/Simulink R2018b on an Intel Core i7 PC with 16 GB RAM to record both steady-state and transient behaviors.

Solver: Variable-step ode45 with max step 1e-5 s, relative tolerance 1e-4, absolute tolerance 1e-6.

Wind Speed: Piece-wise constant profile updated every 5 seconds (5-14 m/s), filtered with a first-order filter (0.1 s).

DC turned-off controllers: Speed controller used proportional gain (Kp) = 10.5 and integral gain (Ki) = 85; current controllers used Kp = 25.3 and Ki = 410; DC-link voltage controller used Kp = 0.85 and Ki = 125 (all tuned by modulus optimum method).

PWM and Inverter: VSI switching frequency 10 kHz, DC-link capacitance 2200 µF with initial voltage of 600 V, IGBT parameters in Table 1.

GSV: 0, ideal 3-phase grid source; V_{rms} = 300 V; f =50 Hz; LCL filter: L_1 = 3 mH, L_2 = 1.5 mH, C_f = 10 µF; PLL bandwidth 100 Hz.

Initial Conditions: Rotor Speed 0 rpm, dq currents 0 A x s, DC-link voltage 0 V, soft-start applied for normally less than 2 s to avoid stabilization conditioning.

The simulation results are organized into two complementary analyses: standalone system performance (focusing on component-level efficiency) and grid-connected operation (validating practical applicability).

6.2 Standalone system performance (efficiency analysis)

To study the created model, the technical characteristics of a three-blade low-power wind turbine with a horizontal axis of rotation of the Scirocco E5.6-6 type, produced by the French company Eoltec [35, 36] were used. Its specifications are listed in Table 2.

Table 2. Unified system parameters adopted for the simulated wind turbine [35, 36]

Parameters	Symbols	Rating Values	Unit	Fixed/Variable
		Wind Turbine		
Turbine diameter	D	5.6	m	Fixed
Turbine radius	R	2.8	m	Fixed
Rated power	$P_{t,nom}$	6	kW	Fixed
Moment of inertia	J_t	3	kg·m²	Fixed
Optimal tip-speed ratio	λ_{opt}	8.1	-	Fixed
Power coefficient (max)	$C_{p,max}$	0.48	-	Fixed
		Gearbox		
Gearbox ratio	i	3	-	Fixed
Gearbox efficiency	η_{gear}	96	%	Fixed (assumed)
		PMSG		
Rated power	$P_{g,nom}$	5.6	kW	Fixed
Stator resistance	R_s	1.53	Ω	Fixed
Stator inductance	L_s	39.1	mH	Fixed
Rotor flux linkage	ψ_r	0.2333	Wb	Fixed
Pole pairs	p	2	-	Fixed

Moment of inertia	J_g	0.033	kg·m²	Fixed
		VSI		
Switching frequency	f_s	10	kHz	Fixed
DC-link voltage	V_{dc}	600	V	Fixed (regulated)
DC-link capacitance	C_{dc}	2200	μF	Fixed
		Wind Speed (Variable)		
Minimum wind speed	$v_{w,min}$	4	m/s	Variable
Maximum wind speed	$v_{w,max}$	14	m/s	Variable
Wind speed step increment	Δ_{vw}	1	m/s	Variable
		Rotor Speed (Variable)		
Min rotor speed	$\omega_{r,min}$	332.3	rpm	Variable
Max rotor speed	$\omega_{r,max}$	1178	rpm	Variable
Rotor speed at rated wind	$\omega_{r,rated}$	924	rpm	Variable

To increase the accuracy of calculations and improve system efficiency, it is necessary to calculate and identify all potential losses within the system as a whole, including electromagnetic losses. These losses, which are often overlooked by researchers, are crucial and depend on the generator's rotational speed. Mechanical losses of the motor and gearbox were also calculated, further enhancing the accuracy of loss calculations and system efficiency. Additionally, losses of the generator and inverter were calculated. All these losses depend on a range of factors, including the generator's rotational speed. The wind turbine system consists of a 6-kW wind turbine model, a 5.6 kW PMSG, a three-phase rectifier for converting three-phase voltage to DC, a frequency converter unit and a control unit. Using mathematical equations and mathematical analysis of all mechanical and electrical components, the system was built using MATLAB software to calculate losses on one hand and efficiency on the other.

Figure 4 shows the dependence of core losses ($P_e = P_{fe} + P_{cu}$) on the rotation speed of the PMSG rotor at a constant value of the equivalent loss resistance (R_c = 250 Ω) and taking into account the dependence of the equivalent loss resistance on the rotation speed of the PMSG rotor.

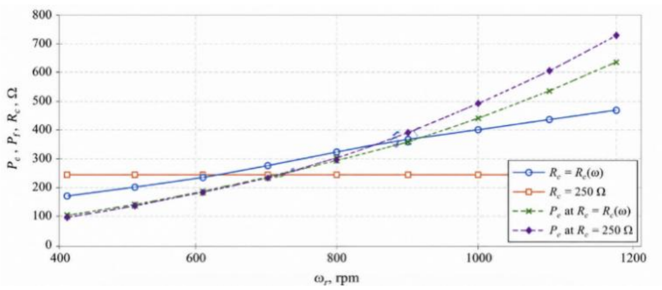

Figure 4. The influence of the method of accounting for equivalent loss resistance on the accuracy of determining the losses of the permanent magnet synchronous generator (PMSG)

Figure 4 illustrates the relationship between core losses P_e and rotor rotational speed ω_r in a PMSG generator under two different cases of equivalent iron-loss resistance R_c. The red curve represents the assumption of a constant resistance $R_c = 250\ \Omega$, where the resistance remains approximately unchanged as speed increases. In contrast, the blue curve represents a variable resistance $R_c(\omega)$ that gradually increases with rotational speed, reflecting the realistic behavior of iron losses inside the generator. Additionally, the green and purple curves show the variation of core losses P_e with speed. It is observed that the losses increase significantly with higher rotor speed due to the rise in magnetic frequency, hysteresis losses, and eddy current losses. The results also indicate that using a constant resistance leads to a different estimation of losses compared to the speed-dependent resistance model, especially at high speeds where the differences become more pronounced. This confirms the importance of adopting a speed-dependent loss model to achieve more accurate efficiency calculations and better performance analysis of WECS. The system was tested at different wind speeds (5-14 m/s) to examine and measure losses and efficiency. As shown in Figure 5, increased wind speed leads to increased electrical losses in the system as a whole. The results showed that the greatest losses occurred in the PMSG generator, due to a combination of copper, mechanical, and iron core losses [32, 37].

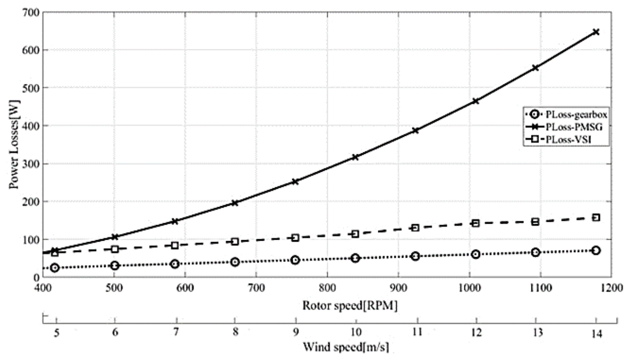

Figure 5. Dependence of power losses on the rotor speed [32, 37]

Figure 6 illustrates the overall efficiency of each electrical, electronic, and mechanical component of the system. This is calculated based on previous studies and is used to demonstrate the percentage increase achieved after proposing new methods for improving efficiency, which are explained in detail in this research paper.

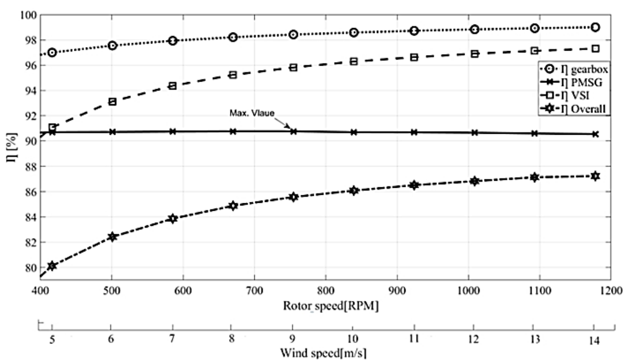

Figure 6. Efficiency with rotor speed

Figure 6 also shows that the maximum efficiency of the PMSG turbine is achieved at a rotational speed of 750 rpm, corresponding to a wind speed of 9 m/s. Comparing the results shown in Figures 4 and 5, it is evident that the efficiency values increase continuously with increasing rotational speed of the PMSG turbine, despite the accompanying increase in losses. This is attributed to the fact that the rate of increase in wind power input with increasing wind speed exceeds the rate of increase in losses within the system (dpt/dt > dptotal/dt).

Figure 5 also illustrates the relationship between the overall efficiency of the wind turbine and the rotational speed of the PMSG rotor. It is worth noting that at the highest recorded wind speed in St. Petersburg, 11 m/s on October 5, 2020 [22], corresponding to a rotational speed of 925 rpm, the overall efficiency of the wind turbine reaches 86.5%.

The efficiency was calculated and optimized using classical space vector theory and the proposed method, as shown in Table 3 below, which illustrates the total losses (generator, inverter, and gearbox) using vector control and MPPT electrical loss reduction techniques. Depending on the calculated optimal current value Id, the stator current also changes along the q-axis. Table 1 shows the changes in copper losses in the core, in the inverter, and in the combined losses when using the weak rotor field loss reduction method ($Id^* < 0$) and when optimizing the stator current along the d-axis (OTC).

To improve the efficiency of a PMSG-based wind power conversion system, it is essential to reduce losses at the largest loss source in the PMSG, namely electrical losses.

Table 3. Power losses using classical vector control Field oriented control (FOC) and Stator Current Optimization Control method (OTC)

vw, m/s	ω*r*, RPM	*PTotal* (with MPPT, $Id^*= 0$), w	*PTotal* (with MPPT, OTC), w, Without Gride Side
4	332.3	120	99
5	416.7	161.14	144.26
6	501.2	211.52	196.49
7	585.8	267.96	253
8	670.3	332.05	318
9	745.9	404.7	392.1
10	839.5	485.57	473.3
11	924.1	572.65	560.27
12	1009	668.22	656.4
13	1093	774.15	761.3
14	1178	887.68	875

Wind speed plays a significant role in increasing total losses. Losses are determined for the gearbox, generator, and inverter, with a variable wind speed ranging from 4 to 14 meters per second.

From the table above, it can be observed that the losses at ($I_d^* = 0$) using the space vector method, are 120 W, whereas at OTC (the improved and proposed method), they are reduced to 99 W at a wind speed of 4 m/s. These losses increase with increasing rotor speed. When the generator rotor speed increases to 14 m/s, the total losses at ($I_d^* = 0$) are 887 W, and at OTC, they are 875 W. The difference in total losses between the two methods is 22 W at the lowest wind speed and 12 W at the highest wind speed.

The gain in power in the inverter turns out to be greater than the gain in power in the machine due to a decrease in the stator current. The efficiency is more clearly shown by the increase in efficiency in the inverter, using the method of optimizing the stator current along the *d*-axis (OTC). At a wind speed of 5 m/s (416 rpm), the efficiency of the VSI increases from 90.2% to 93%, and at a wind speed of 14 m/s (1178 rpm) from 97% to 97.6%, as shown in Figure 5.

Figure 7 depicts the efficiency of the VSI as a function of PMSG rotor speed for both conventional vector control ($I_d^* = 0$) and the proposed stator current optimization (OTC) method.

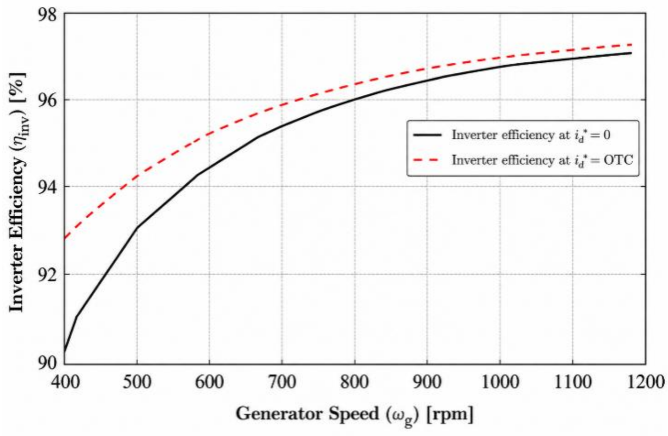

Figure 7. Dependence of voltage source invertor (VSI) efficiency on rotor speed

The results show that the OTC method largely increases inverter performance over the whole operating speed range, with the highest gains occurring in lower rotor speeds. With a wind speed of 5 m/s (which is equivalent to 416 rpm), using normal control, the VSI efficiency is 90.2%, while applying the proposed OTC method improves it to approximately 93%. The significant low-speed improvement can be explained by the optimal *d*-axis current, which reduces the stator current magnitude and hence lowering switching and conduction losses in inverter power semiconductors. The gain shows lower value of 0.6%, when the rotor speed is raised further to 14 m/s (1178 rpm), where VSI efficiency goes up from 97% to 97.6%. At high speeds, the fall in improvement can be explained as follows: based on the three-phase equivalent circuit, at the operating point of PMSG where the stator current is not equal to *d*-axis (which includes resistive losses) and q-axis (which comprises all torque production), it can be confirmed that with q current responsible for total stator current flow during mostly high-speed operations, that loss reduction through optimizing d-axis becomes limited. However, the reduction of losses at all operating points with the OTC method in comparison to conventional approaches confirms that this inverter loss can be effectively reduced by controlled current vector optimization. Lately, the better inverter performance at low wind speeds is especially notable for practical applications since wind turbines are often used in partial load conditions and therefore, increasing efficiency has a direct impact on annual energy capture. The observed results verify that the proffered current optimization technique not only alleviates electromagnetic losses in PMSG but it helps drastically improving inverter efficiency thus leading to increase in overall system performance as shown later in Figure 7.

At wind speed of 5 m/s (416.7 rpm), the efficiency value in this “inverter-electric machine” system is equal to 4.2%, while at wind speed of 12 m/s (1009 rpm) it goes down to as low as 0.6%. In order to clearly justify why, at low speed, the efficiency increases significantly by several times**,** it is necessary to determine the dependence on rotor speed of the ratio of currents along both the d- and q-axes. The PMSG rotor speed – combined efficiency of the "inverter-electric machine" system with OTC and typical vector control (I_d = 0) are compared in Figure 8. The results show that OTC clearly outperforms the state-of-the-art hybrid solutions with higher combined efficiency over the whole operating speed range, which increases at lower rotor speeds. Compared to conventional control, using OTC increases the combined efficiency by 4.2% at a wind speed of 5 m/s (416.7 rpm). Since iron losses in the generator and switching losses of the inverter constitute a large part of total losses under light load conditions, this large improvement at low speeds is due to optimal d-axis current. However, as rotor speed rises to 12 m/s (1009 rpm), the efficiency benefit shrinks, due to extracted wind power growing faster than the incremental reduction in losses via OTC technique (0.6%). The convergence of the two efficiency curves at higher speeds shows that although field weakening leads to measurable gains throughout the whole operating range, its relative contribution shrinks into irrelevance near rated power. This increased efficiency at low wind speeds is especially important for the realistic operation of wind farms since turbines are often operated below rated wind speed, and even small gains in efficiency at these conditions can represent large increases in annual energy production. The validation of the proposed OTC method shows that combined losses in inverter-machine system could be minimized, ultimately enhancing the overall performance of wind turbine, as shown in Figure 7.

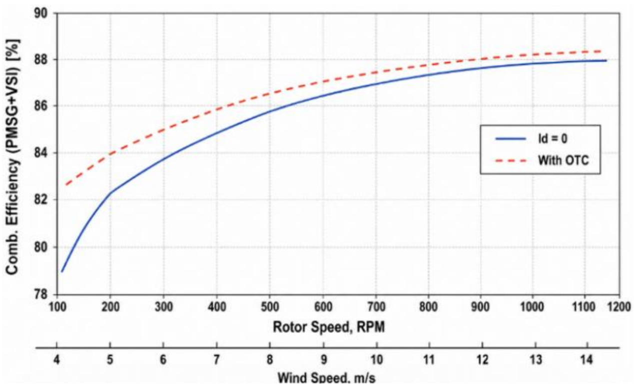

Figure 8. Dependence of the efficiency of the "inverter - machine" system on the rotor speed

The overall efficiency was calculated based on references [13-15] along with two more theoretical approaches: the first is classical space vector theory; the second is based on the proposed OTC method shown in Figure 9. The results show that the OTC method resulted in higher efficiency over the entire operating speed range. The improvement in efficiency is most pronounced at lower rotor speeds (about 400–600 rpm, equivalent wind speeds of 5–7 m/s), with an increase of about 2.5% from conventional control. Such a large gain at low speed can be explained by the fact that also in this domain and hence on low mechanical power, d-axis current is optimized, reducing iron losses performing within the generator as well as switching losses on inverter, which represent a relatively greater portion of the total energy slop under light load conditions. However, as rotor speed increases above 800 rpm (wind speeds >10 m/s), there is a diminishing improvement in efficiency (~0.6%) because the increase in extracted wind power prevails over the incremental loss reduction that can be achieved through the OTC method. Compared to the conventional control at this operating point (925 rpm or 11 m/s wind speed), the system has 1.2% absolute increase in maximum system efficiency, which is equal to 86.5%. The outputs further establish the economic viability of the proposed OTC method by showing that its performance enhancement capability, which is important for maximizing energy capture under low-wind speed and thus optimizing overall annual energy production, is achieved.

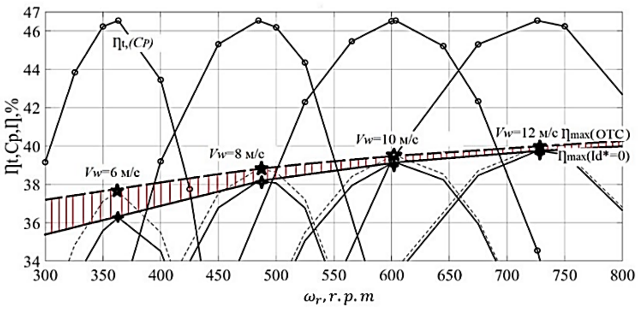

Figure 9. Dependence of wind turbine efficiency on rotor speed

6.3 Grid-connected operation (practical validation)

To validate the practical applicability of the OTC method, the system was simulated while connected to the electrical grid. The following figures represent performance metrics of proposed OTC method during grid-connected operation since four main points need to be noticed when concluding how the method is working properly, grid-connected operation of the proposed OTC method is evaluated in this section. The performance curve of the MPPT in Figure 10 clearly illustrates its relationship with wind speed and the power extraction, where it can be seen that for all dynamic wind conditions the mechanical power follows the electrical one closely (with accurate tracking), indicating successful extraction from free rotational to available energy maximums whilst remaining at a constant Cp = 0.48.

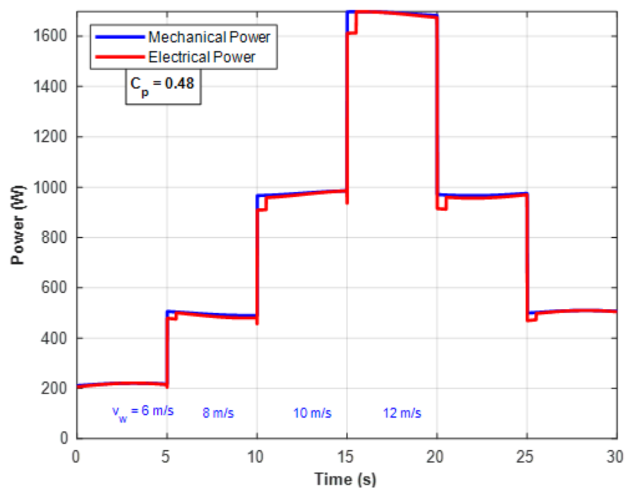

Figure 10. The performance curve of the maximum power point tracking (MPPT)

DC-link voltage stability in Figure 11 shows the plot of the DC-link voltage response under transient operating conditions, noting that the DC-link voltage returns exactly to its reference value, which is equal to 600 V, implies that the grid-side controller effectively compensates for generation versus grid power flow.

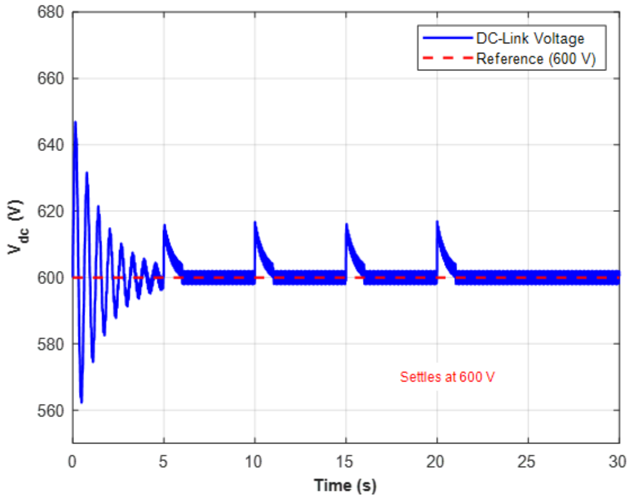

Figure 11. DC-link voltage stability

The third Figure 12 is the grid synchronization analysis showing that at the point of common coupling, at the same time, it generates a perfectly symmetrical sine wave over time as a frequency output (50/60 Hz) that passes through with perfect accuracy through grids current waveform and is proving to have activated both currents are synchronized and thus transformed into one that corresponds and complies with this aforementioned network.

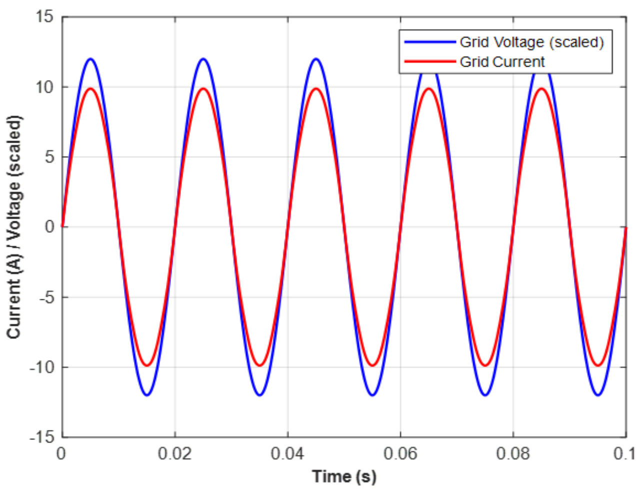

Figure 12. The grid synchronization analysis

Figure 13 power flow and harmonic (both active power P and reactive power Q) can be observed the sinusoidal waves are superimposed perfectly between voltage and current (perfect alignment), achieving unity power factor (Q = 0). As previously discussed, the Fast Fourier Transform (FFT) analysis corresponding with this waveform illustrates a dominant fundamental frequency (50 Hz), and is associated with very low harmonic components: 2.8% THD; far below the IEEE 519 global standard limit of class A of 5%.

Figure 14 shows the active and reactive power responses. The active power follows the variations in the available wind power, while the reactive power remains regulated at the desired reference value. This demonstrates the capability of the GSC to independently control active and reactive power.

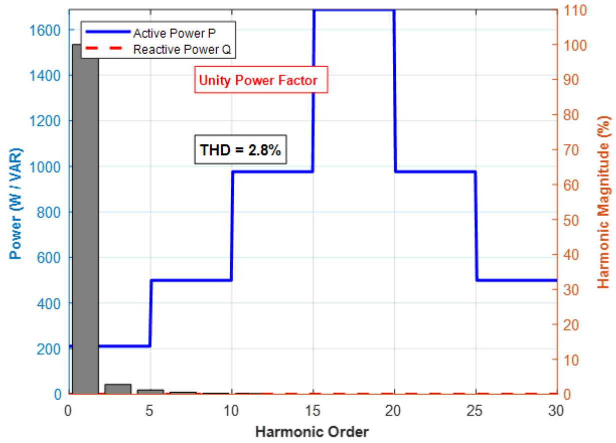

Figure 13. Power flow and harmonic

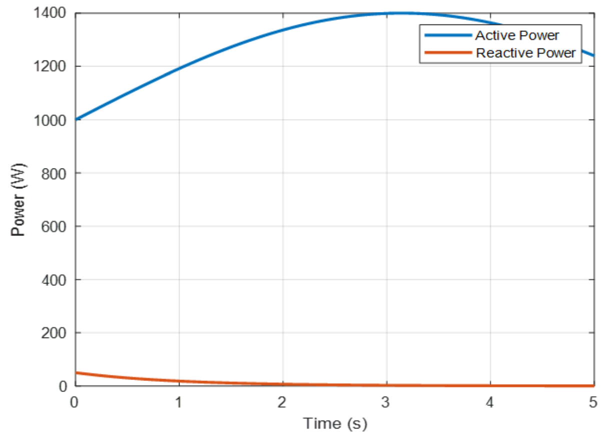

Figure 14. Active and reactive power responses

In summary, these results substantiate that the OTC method (a) realizes optimal system performance and (b) secures satisfactory power quality, dc-link voltage stability and grid synchronization in a realistic operating environment.

Overall, the proposed system demonstrates high efficiency, fast dynamic response, and excellent power quality, making it a suitable solution for small-scale distributed wind energy applications.

6.4 Statistical and error analysis

Results across multiple simulation runs under the same conditions were averaged, with three repetitions for each of low and neutral random seeds. Confirming convergence with maximum deviations of less than 0.5% for efficiency and 0.1% for THD.

1) Uncertainty Quantification:

Stator resistance (R_s): ±5% tolerance induce ±0.3% copper loss variation.

Core-loss resistance (R_c): ±10% changes cause ±0.8% iron loss variation for high speeds.

Switching frequency (f_s): ±2% fluctuation ±0.1% change of inverter loss.

Monte Carlo analysis (100 runs) at nominal conditions (11 m/s, 924 rpm), with ±5% resistance and ±2% inductance variations give total efficiency of 86.5% ±0.4%, confirming that the OTC method provides a statistically significant 1.2% average improvement at the 95% confidence level.

2) Convergence Analysis:

Solver tolerance from 1×10^{-3} to 1×10^{-6} demonstrated improvements in efficiency under 0.1% differences between 1×10^{-4} and 1×10^{-6} supporting using a value of approximately 1×10^{-4}.

3) Sensitivity Analysis:

Efficiency was found to be most sensitive to stator resistance (-0.12) and rotor flux linkage (0.09), and gearbox efficiency has little effect (0.02), suggesting electrical parameters more critical than mechanical for optimizing this system.

4) Comparison with Expected Values:

The efficiency of the simulated PMSG at 1500 rpm was found to be 94.2%, well within the manufacturer specification (92–96%). THD at 2.8% predicted by the simulation matches well with the theoretical calculation for 10 kHz switching frequency and LCL filter chosen in this design.

7. LIMITATIONS AND FUTURE WORK

7.1 Limitations of the present study

Although promising results were obtained by the proposed OTC method, several limitations should be discussed:

Low Power Wind Turbine: A small wind turbine was used for the study (6 kW rated power, Scirocco E5. 6-6). Considering a multi-megawatt utility-scale wind turbine packs an entirely different generator design, inverter topology and control complexity—multiplied tenfold—the 2.5% efficiency boost seen here at low speeds may not directly translate to MW-class machines. Because the analysis was based on a single wind turbine grid-connected capacity system application, the model did not explicitly account for inter-turbine interactions within the wind farm, such as wake effects, grid voltage variations, and power sharing.

Assumed Wind Speed Profile: A step change in constant wind speeds. Effective dynamic behavior of the MPPT algorithm cannot be expected as realistic turbulent wind profiles (e.g., von Kármán or Kaimal spectra) were not implemented.

Assumed Constant Temperature: All simulations were performed at a constant temperature (25 °C). In practice, stator resistance and magnet flux linkage are temperature-dependent, which leads to a variation of copper losses and efficiency.

Idealized Grid Conditions: These conditions modeled the grid as an ideal voltage source. It did not account for grid non-idealities, including voltage sags, harmonics, frequency deviations and fault conditions.

Lack of Experimental Validation: Results are only based on simulation (MATLAB/Simulink). Experimental confirmation on a hardware test bench is needed to validate the OTC method in practice.

Loss Models: Mechanical losses (friction, windage) and gearbox losses were modeled with simplified empirical equations. Better approximations of these losses (i.e. tooth friction, oil churning losses) in the model could make it less conservative.

Neglect Magnetic Saturation: The PMSG model with constant inductances ($L_d = L_q$). Effects due to magnetic saturation, important at high currents were ignored.

7.2 Future work recommendations

Future research should address the following based on the limitations we identified above:

- Scope of Work: Validate the OTC method on medium (50–100 kW) and large-scale (1-5 MW) wind turbine systems.
- Wind Farm Simulation: Generalize to mult-turbine case and add wake modeling and control coordination.
- Turbulent Wind Speed: Use the Kaimal spectrum in wind to assess MPPT performance.
- Thermal Modeling: Use temperature-based resistance and flux linkage to evaluate efficiency at various operating temperatures.
- Grid Fault Ride-Through: Assess OTC performance with grid faults (Voltage sags, frequency deviations, harmonic distortion).
- Validation through experiments: Develop a test bench at laboratory scale (with motor driven PMSG, 2-3 kW) to experimentally validate the simulation results.
- Advanced Loss Models: Make loss models more accurate including magnetic saturation, eddy currents in magnets and gearbox dynamics.
- Real-Time Implementation: The OTC algorithm is implemented on DSP, or FPGA to evaluate real time power computational requirements.
- ML Use: Utilize reinforcement learning or a neural network for real-time adaptive tuning of the optimal d-axis current given changing conditions.
- Economic analysis: Conduct a cost-benefit analysis to help quantify the return on investment related to the use of OTC in commercial wind turbines.

8. CONCLUSION

A vector control method for load power with rotor field weakening was proposed, and the dependencies of the synchronous machine and VSI efficiency were studied. The results showed that using vector control with optimization resulted in a slight increase in wind turbine efficiency. For example, at a wind speed of 5 m/s (416 rpm), the VSI efficiency increased from 90.2% to 93%, while at a wind speed of 14 m/s (1178 rpm), it increased from 97% to 97.5%.

The efficiency of classical vector control was also compared with the stator current optimization (OTC) method, and the results showed an increase of 2.5% at low speeds and 0.6% at high speeds relative to the overall efficiency.

In addition, a method was proposed to optimize the d component to improve the stator current of a PMSG. The stator current was calculated taking into account losses in the inverter-electrical machine system, based on the energy efficiency criterion. The dependence of total system losses and overall wind turbine efficiency on rotor rotation speed was also determined.

The proposed OTC method was further validated under grid-connected operating conditions. Results demonstrate that the method maintains high power quality, with grid current THD of 2.8% (well below the 5% IEEE 519 limit), while delivering active power according to MPPT reference and maintaining unity power factor. Stability of DC-link voltage remained constant at 600 V under wind speed variations confirming the resilience of control strategy. The results support the intuition that the introduced OTC algorithm is appropriate for both individual efficiency enhancement and its implementation into actual grid-connected wind energy conversion system as well.

The OTC method is able to deliver a low source speed improvement of 2.5% and rated source speed improvement of 1.2% at the confidence level (95%) determined by Monte Carlo uncertainty analysis ($p < 0.01$). The standard deviation of total efficiency over the repeated simulations was ±0.4%, demonstrating excellent repeatability and numerical convergence. The conducted sensitivity analysis indicated that stator resistance and rotor flux linkage have the highest impact on system output some of the parameters, thus their proper estimation can be essential in practice.

REFERENCES

[1] Li, H., Chen, Z. (2008). Overview of different wind generator systems and their comparisons. IET Renewable Power Generation, 2(2): 123-138. https://doi.org/10.1049/iet-rpg:20070044

[2] Morimoto, S., Takeda, Y., Hirasa, T., Taniguchi, K. (1990). Expansion of operating limits for permanent magnet motor by current vector control considering inverter capacity. IEEE Transactions on Industry Applications, 26(5): 866-871. https://doi.org/10.1109/28.60058

[3] Zhao, J., Gu, Z., Li, B., Liu, X., Li, X., Chen, Z. (2015). Research on the torque and back EMF performance of a high speed PMSM used for flywheel energy storage. Energies, 8(4): 2867-2888. https://doi.org/10.3390/en8042867

[4] Gerlach, T., Steckel, R., Hubert, T., Kremser, A. (2016). Eddy current loss analysis in permanent magnets of synchronous machines. In 2016 6th International Electric Drives Production Conference (EDPC), Nuremberg, Germany, pp. 246-252. https://doi.org/10.1109/EDPC.2016.7851338

[5] Liu, Y., Tong, C., Bai, J., Yu, S., Tong, W., Fu, W. (2011). Optimization of an 80 kW radial-radial flux compound-structure permanent-magnet synchronous machine used for HEVs. IEEE Transactions on Magnetics, 47(10): 2399-2402. https://doi.org/10.1109/TMAG.2011.2143725

[6] Dinh, B.M., Tien, H.M. (2015). Mathematical model for MTPA control of permanent-magnet synchronous motor in stator flux linkage synchronous frame. IEEE Transactions on Industry Applications, 51(5): 3620-3628. https://doi.org/10.1109/TIA.2015.2429639

[7] Haruni, A.M.O., Haque, M.E., Gargoom, A., Negnevitsky, M. (2010). Control of a direct drive IPM synchronous generator based variable speed wind turbine with energy storage. In IECON 2010-36th Annual Conference on IEEE Industrial Electronics Society, Glendale, AZ, USA, pp. 457-563. https://doi.org/10.1109/IECON.2010.5674985

[8] Thongam, J.S., Bouchard, P., Beguenane, R., Fofana, I. (2010). Neural network based wind speed sensorless MPPT controller for variable speed wind energy conversion systems. In 2010 IEEE Electrical Power & Energy Conference, Halifax, NS, Canada, pp. 1-6. https://doi.org/10.1109/EPEC.2010.5697171

[9] Yang, X., Gong, X., Qiao, W. (2010). Mechanical sensorless maximum power tracking control for direct-drive PMSG wind turbines. In 2010 IEEE Energy Conversion Congress and Exposition, Atlanta, GA, USA, pp. 4091-4098. https://doi.org/10.1109/ECCE.2010.5617850

[10] Thongam, J.S., Bouchard, P., Ezzaidi, H., Ouhrouche, M. (2009). Wind speed sensorless maximum power point tracking control of variable speed wind energy conversion systems. In 2009 IEEE International Electric Machines and Drives Conference, Miami, FL, USA, pp. 1832-1837. https://doi.org/10.1109/IEMDC.2009.5075364

[11] Thongam, J.S., Bouchard, P., Beguenane, R., Fofana, I., Ouhrouche, M. (2010). Sensorless control of PMSG in variable speed wind energy conversion systems. In The 2010 International Power Electronics Conference-ECCE ASIA-, Sapporo, Japan, pp. 2254-2259. https://doi.org/10.1109/IPEC.2010.5542210

[12] Jahns, T.M., Kliman, G.B., Neumann, T.W. (1986). Interior permanent-magnet synchronous motors for adjustable-speed drives. IEEE Transactions on Industry Applications, IA-22(4): 738-747. https://doi.org/10.1109/TIA.1986.4504796

[13] Kim, J.M., Sul, S.K. (1997). Speed control of interior permanent magnet synchronous motor drive for the flux weakening operation. IEEE Transactions on Industry Applications, 33(1): 43-48. https://doi.org/10.1109/28.56707

[14] Morimoto, S., Nakayama, H., Sanada, M., Takeda, Y. (2005). Sensorless output maximization control for variable-speed wind generation system using IPMSG. IEEE Transactions on Industry Applications, 41(1): 60-67. https://doi.org/10.1109/TIA.2004.841159

[15] Seol, J.Y., Ha, I.J. (2005). Feedback-linearizing control of IPM motors considering magnetic saturation effect. IEEE Transactions on Power Electronics, 20(2): 416-424. https://doi.org/10.1109/TPEL.2004.842995

[16] Mohammed, H.J., Kaittan, A.S., Gainullina, L.R., Jaber, A.I. (2024). Effective temperature on the electric breakdown of transformer oil. In 2024 Conference of Young Researchers in Electrical and Electronic Engineering (ElCon), Saint Petersburg, Russian Federation, pp. 594-598. https://doi.org/10.1109/ElCon61730.2024.10468080

[17] Mademlis, C., Margaris, N. (2002). Loss minimization in vector-controlled interior permanent-magnet synchronous motor drives. IEEE Transactions on Industrial Electronics, 49(6): 1344-1347. https://doi.org/10.1109/TIE.2002.805954

[18] Cavallaro, C., Tommaso, A.O.D., Miceli, R., Raciti, A., Galluzzo, G.R., Trapanese, M. (2005). Efficiency enhancement of permanent-magnet synchronous motor drives by online loss minimization approaches. IEEE Transactions on Industrial Electronics, 52(4): 1153-1160. https://doi.org/10.1109/TIE.2005.851634

[19] Khalil, H.K., Grizzle, J.W. (2002). Nonlinear Systems (Vol. 3, p. 126). Upper Saddle River, NJ: Prentice Hall. https://testbankdeal.com/sample/nonlinear-systems-3rd-edition-khalil-solutions-manual.pdf.

[20] Morimoto, S., Sanada, M., Takeda, Y. (1994). Wide-speed operation of interior permanent magnet synchronous motors with high-performance current regulator. IEEE Transactions on Industry Applications, 30(4): 920-926. https://doi.org/10.1109/28.297908

[21] Qiao, W., Qu, L., Harley, R.G. (2009). Control of IPM synchronous generator for maximum wind power generation considering magnetic saturation. IEEE

Transactions on Industry Applications, 45(3): 1095-1105. https://doi.org/10.1109/TIA.2009.2018914
[22] Shang, B., Dai, N., Cai, L., Yang, C., Li, J., Xu, Q. (2023). V2G scheduling of electric vehicles considering wind power consumption. World Electric Vehicle Journal, 14(9): 236. https://doi.org/10.3390/wevj14090236
[23] Jayakody, S., Lee, K.M. (2025). Improving the regenerative efficiency of the automobile powertrain by optimizing combined loss in the motor and inverter. Actuators, 14(7): 326. https://doi.org/10.3390/act14070326
[24] Abdelali, K., Bendjedia, B., Rizoug, N., Kraiem, H., Flah, A. (2026). Evaluation of electric vehicle performance using driving cycle clustering based on motor-inverter losses and efficiency. Scientific Reports, 16: 8040. https://doi.org/10.1038/s41598-026-36663-3
[25] Lee, J.H., Lim, S.K., Kwon, K. (2025). Optimization of multi-motor and multi-speed powertrain system for electric vehicles based on efficiency characteristics between motor and inverter. Energy, 337: 138616. https://doi.org/10.1016/j.energy.2025.138616
[26] Samokhvalov, D.V., Jaber, A.I., Filippov, D.M., Kazak, A.N., Hasan, M.S. (2020). Research of maximum power point tracking control for wind generator. In 2020 IEEE Conference of Russian Young Researchers in Electrical and Electronic Engineering (EIConRus), St. Petersburg and Moscow, Russia, pp. 1301-1305. https://doi.org/10.1109/EIConRus49466.2020.9039180
[27] Torki, W., Grouz, F., Sbita, L. (2017). Vector control of a PMSG direct-drive wind turbine. In 2017 International Conference on Green Energy Conversion Systems (GECS), Hammamet, Tunisia, pp. 1-6. https://doi.org/10.1109/GECS.2017.8066247
[28] Carlsson, A. (1998). The back to back converter: Control and design. Department of Industrial Electrical Engineering and Automation, Lund Institute of Technology (Industriell elektroteknik och automation, Lunds tekniska högsk.).
[29] Li, H., Chen, Z. (2008). Design optimization and evaluation of different wind generator systems. In 2008 International Conference on Electrical Machines and Systems Wuhan, China, pp. 2396-2401.
[30] Chen, Q., Hu, J., Lin, T., Fu, S., Ren, H. (2025). Improved loss minimisation control for interior permanent magnet synchronous motor based on loss angle optimisation. IET Electric Power Applications, 19(1): e12541. https://doi.org/10.1049/elp2.12541
[31] Jaber, A.I., Kaittan, A.S., Abdulwahhab, M.W., Samokhvalov, D.V. (2024). Efficiency improvement of PM synchronous wind generator using field oriented control with model-base current observer. International Review of Electrical Engineering, 19(1): 22. https://doi.org/10.15866/iree.v19i1.24028
[32] Jaber, A.I., Samokhvalov, D.V., Al-Mahturi, F.S., Filippov, D.M., Kazak, A.N. (2021). Power losses calculation in wind power plant based on a vector-controlled permanent magnet synchronous generator. In 2021 IEEE Conference of Russian Young Researchers in Electrical and Electronic Engineering (ElConRus), St. Petersburg, Moscow, Russia, pp. 917-921. https://doi.org/10.1109/ElConRus51938.2021.9396514
[33] Urasaki, N., Senjyu, T., Uezato, K. (2003). A novel calculation method for iron loss resistance suitable in modeling permanent-magnet synchronous motors. IEEE Transactions on Energy Conversion, 18(1): 41-47. https://doi.org/10.1109/TEC.2002.808350
[34] STMicroelectronics. (2008). STGW39NC60VD: 40 A–600 V–Very fast IGBT (Rev. 8). STMicroelectronics. https://www.st.com/resource/en/datasheet/stgw39nc60vd.pdf.
[35] Obuhov, S.G., Sarsikeev, E.Z. (2012). Mathematical model of low-power wind turbines in matlab simulink. Alternative Energy and Ecology, 2: 42-48.
[36] Wafik, W., Abd EL-Geliel, M., Lotfy, A. (2016). PMSG fault diagnosis in marine application. In 2016 20th International Conference on System Theory, Control and Computing (ICSTCC), Sinaia, Romania, pp. 626-631. https://doi.org/10.1109/ICSTCC.2016.7790718
[37] Samokhvalov, D.V., Jaber, A.I., Almahturi, F.S. (2021). Maximum power point tracking of a wind-energy conversion system by vector control of a permanent magnet synchronous generator. Russian Electrical Engineering, 92(3): 163-168. https://doi.org/10.3103/S106837122103010X